

Electronic supplementary information (ESI)

Coordination polymers with pyridyl-salen ligand for photocatalytic carbon dioxide reduction

Yi Liu, Jin-Han Guo, Xiao-Yao Dao, Xiu-Du Zhang, Yue Zhao and Wei-Yin Sun*

Coordination Chemistry Institute, State Key Laboratory of Coordination Chemistry, School of Chemistry and Chemical Engineering, Nanjing National Laboratory of Microstructures, Collaborative Innovation Center of Advanced Microstructures, Nanjing University, Nanjing 210023, China.

* Corresponding author.

Email address: sunwy@nju.edu.cn (W. Y. Sun).

Materials and methods. All commercially available chemicals and solvents are of reagent grade and were used as received without further purification. Powder X-ray diffraction (PXRD) data were collected on a Bruker D8 Advance X-ray diffractometer with Cu K α ($\lambda = 1.5418 \text{ \AA}$) radiation. Cyclic voltammetry curves were obtained by using a CHI 730E electrochemical analyzer (CH Instruments, Inc., Shanghai). Electrospray ionic mass spectrometry (ESI-MS) data were collected on a ThermoFisher Scientific LCQ Fleet instrument. FT-IR spectra (KBr disk) were obtained on a Bruker Vector 22 FT-IR spectrophotometer in the range of 400 - 4000 cm^{-1} . EPR spectra were obtained using a Bruker EMX plus-6/1 variable temperature X-band apparatus at 90 K and simulated with the software of WINEPR SimFonia. X-ray photoelectron spectroscopy (XPS) was performed on a UIVAC-PHI 5000 VersaProbe using monochromatized Al K α at $h\nu = 1486.6 \text{ eV}$. The C 1s

peak was used as the reference peak. Elemental analyses (EA) for C, H, and N were performed on a PerkinElmer 240C elemental analyzer. UV-vis diffuse reflectance data were recorded on a Shimadzu UV-3600 spectrophotometer in the wavelength range of 400-1200 nm, a white standard of BaSO₄ was used as reference. The UV-vis spectral upon electrochemical reduction were performed on a Pine Research Honeycomb Spectroelectrochemical Cell. Thermogravimetric analyses (TGA) were carried out under nitrogen atmosphere with a heating rate of 10 °C min⁻¹ on a Mettler-Toledo (TGA/DSC1) thermal analyzer.

Synthesis of ligand H₂L. A mixture of 2-hydroxy-4-(pyridin-4-yl)benzaldehyde (1.00 g, 5.0 mmol) and ethane-1, 2-diamine (0.15 g, 2.5 mmol) in 20 mL of ethanol was stirred at 85 °C for 8 h. After the mixture was cooled to room temperature, precipitate was filtered and washed with ethanol to provide pure product as yellow solid. ¹H NMR (400 MHz, CDCl₃) δ 13.35 (2H, s), 8.67 (4H, dd, J 4.5, 1.6), 8.44 (2H, s), 7.49 (4H, dd, J 4.5, 1.7), 7.36 (2H, d, J 8.0), 7.23 (2H, d, J 1.7), 7.14 (2H, dd, J 7.9, 1.7), 4.02 (4H, s).

Synthesis of [Mn(L)Cl]·DMF (1). A mixture of H₂L (12.7 mg, 0.03 mmol) and MnCl₂·4H₂O (5.9 mg, 0.03 mmol) in DMF/methanol mixed solvent (5 mL, v/v: 4/1) was heated at 90 °C under autogenous pressure in a glass vial for 50 h, followed by cooling to room temperature. Dark brown crystals of **1** formed in 81% yield. *Anal.* Calc. for C₂₉H₂₇N₅O₃MnCl: C, 59.65; H, 4.66; N, 11.99%. Found: C, 59.71; H, 4.65; N, 12.03%. IR bands (KBr pellet, cm⁻¹, Fig. S2): 3424(w), 1598(s), 1552(w), 1520(w), 1502(w), 1386(s), 1323(w), 1297(w), 1246(w), 1204(w), 1152(w), 1090(w), 1049(w), 943(w), 804(w), 729(w), 631(w), 482(w).

Synthesis of [Fe(L)Cl]·DMF (2). Complex **2** was achieved by the same procedure used for synthesis of **1**, except that FeCl₃·6H₂O (8.1 mg, 0.03 mmol) was used to replace MnCl₂·6H₂O. Block crystals of **2** were achieved in 75% yield. *Anal.* Calc. for

C₂₉H₂₇N₅O₃FeCl: C, 59.56; H, 4.65; N, 11.97%. Found: C, 59.44; H, 4.60. N, 11.93%. IR bands (KBr pellet, cm⁻¹, Fig. S2): 3439(w), 1595(s), 1553(w), 1523(w), 1475(w), 1504(w), 1386(s), 1326(w), 1297(w), 1243(w), 1200(w), 1146(w), 945(w), 802(w), 730(w), 627(w), 455(w).

Photocatalytic conversion of CO₂. Photoreduction of CO₂ was carried out in a solvent-free reaction system (CEL-SPH2N-D9, CeAulight, China) equipped with a circulating water filter to exclude photothermal effect.^{S1} The photocatalyst (2 mg) was dispersed onto a glass fiber film (Φ25 mm, 0.22 μm pore diameter, Xingya, Shanghai) and the film was activated in vacuum at 120 °C for 12 h. Then the film was fixed in the reaction cell and triethanolamine (TEOA) (2 mL) was added into the reactor. After the complete evacuation (no O₂ or N₂ could be detected), the reaction system was infused with 80 kPa pure CO₂ gas (99.999%) and irradiated using a 300 W xenon arc lamp (Sirius-300P, Zolix Instruments Co., Ltd., China) with a 400-780 nm filter (CeAulight, China). The gas products were monitored by using gas chromatography (GC-9860, Luchuang Instrument, China) equipped with TCD and FID detectors.

X-ray crystallography. Crystallographic data for **1** and **2** were collected on a Bruker Smart Apex II CCD single-crystal X-ray diffractometer with a graphite-monochromated Mo Kα radiation ($\lambda = 0.71073 \text{ \AA}$). The integration of the diffraction data and the intensity corrections for the Lorentz and polarization effects was carried out using the SAINT program. Absorption corrections were carried out using SADABS.^{S2} Structures were solved by direct methods with SHELXS and refined by the full-matrix least-squares method using the SHELXL.^{S3, S4} All non-hydrogen atoms were refined on F^2 anisotropically. The hydrogen atoms were calculated geometrically and refined isotropically using the riding model. Crystal data and refinement details of **1** and **2** are given in Table 1, selected bond lengths and angles are listed in Table S2.

Electrochemical characterization.

1) Electrochemical impedance spectroscopy. The electrochemical impedance spectroscopy was performed on a Novocontrol Concept 80 Impedance Tester in the frequency range from 10 Hz to 900 kHz at room temperature. Two stainless steel disc electrodes (2 cm in diameter) were used to sandwich the samples, which were cut into small discs with diameters of 1.3 cm.

2) Photocurrent measurements. Photocurrent measurements were performed on a CHI 730E electrochemical work station (CH Instrument, Shanghai, China) in a standard three-electrode system with a 0.1 M tetrabutylammonium hexafluorophosphate MeCN solution as the electrolyte. The working electrode was prepared by dropping the suspension (250 μ L) onto the surface of the photocatalyst-coated ITO (1 cm²). The counter-electrode was a platinum plate and the reference electrode was an aqueous SCE electrode. And then, the photo-responsive signals of the samples were measured under chopped light at 0.5 V.

3) EPR measurements. Samples was added to mixture containing deionized TEOA and MeCN, then 50-60 μ L above suspension was transferred to the EPR resonator, and degassed by several freeze-pump-thaw procedures and sealed. The same Xe lamp was used in the measurement at room temperature. The solution EPR spectra were obtained using a Bruker EMX plus-6/1 variable temperature X-band apparatus at 90 K and simulated with the software of WINEPR SimFonia.

Computational details. All of the DFT calculations were carried out by using the DMol³ module of Materials Studio 6.0 software (Accelrys Software Inc.). The geometry optimized molecular structures by LDA / PWC basis set and the multiplicity is corrected at auto level. Frequency calculations were carried out to confirm that each structure was a local minimum.

Table S1. Crystal Data and Structure Refinements for **1** and **2**.

Complex	1	2
Chemical formula	C ₂₉ H ₂₇ N ₅ O ₃ MnCl	C ₂₉ H ₂₇ N ₅ O ₃ FeCl
Formula weight	583.94	584.85
Temperature/K	173(2)	293(2)
Crystal system	orthorhombic	orthorhombic
Space group	<i>Pbca</i>	<i>Pbca</i>
<i>a</i> /Å	13.4901(16)	13.4819(5)
<i>b</i> /Å	13.2578(16)	13.3393(5)
<i>c</i> /Å	30.134(4)	30.1323(13)
<i>V</i> /Å ³	5389.5(11)	5419.0(4)
<i>Z</i>	8	8
<i>D_c</i> /g cm ⁻³	1.439	1.434
μ /mm ⁻¹	0.630	0.696
<i>F</i> (000)	2416	2424
Reflections collected	29111	37802
Unique reflections	6320	4767
GOF	1.042	1.238
<i>R</i> ₁	<i>R</i> ₁ = 0.0456	<i>R</i> ₁ = 0.0331
<i>wR</i> ₂ [<i>I</i> > 2σ(<i>I</i>)] ^{<i>a,b</i>}	<i>wR</i> ₂ = 0.1125	<i>wR</i> ₂ = 0.0948
<i>R</i> ₁	<i>R</i> ₁ = 0.0606	<i>R</i> ₁ = 0.0445
<i>wR</i> ₂ (all data)	<i>wR</i> ₂ = 0.1201	<i>wR</i> ₂ = 0.1004

^{*a*} *R*₁ = Σ||*F*_o| - |*F*_c||/Σ|*F*_o|.

^{*b*} *wR*₂ = |Σ*w*(|*F*_o|² - |*F*_c|²)/Σ|*w*(*F*_o)²|^{1/2}, where *w* = 1/[σ²(*F*_o)² + (*aP*)² + *bP*]. *P* = (*F*_o)² + 2*F*_c)²/3.

Table S2 Selected bond lengths (Å) and angles (°)

Compound 1			
Mn(1)-O(1)	1.8974(16)	Mn(1)-O(2)	1.8823(17)
Mn(1)-N(1)	1.9810(2)	Mn(1)-N(2)	1.9957(18)
Mn(1)-N(3)#1	2.4110(2)	Mn(1)-Cl(1)	2.5325(7)
O(1)-Mn(1)-O(2)	94.18(7)	O(1)-Mn(1)-N(1)	91.65(7)
O(1)-Mn(1)-N(2)	171.15(8)	O(1)-Mn(1)-N(3)#1	84.45(7)
O(1)-Mn(1)-Cl(1)	92.31(5)	O(2)-Mn(1)-N(1)	172.98(8)
O(2)-Mn(1)-N(2)	92.01(7)	O(2)-Mn(1)-N(3)#1	86.59(7)
O(2)-Mn(1)-Cl(1)	93.36(5)	N(1)-Mn(1)-N(2)	81.78(8)
N(1)-Mn(1)-N(3)#1	90.08(8)	N(1)-Mn(1)-Cl(1)	90.32(6)
N(2)-Mn(1)-N(3)#1	89.61(8)	N(2)-Mn(1)-Cl(1)	93.64(6)
N(3)#1-Mn(1)-Cl(1)	176.75(5)		
Compound 2			
Fe(1)-O(1)	1.8871(14)	Fe(1)-O(2)	1.9048(14)
Fe(1)-N(1)	2.0967(17)	Fe(1)-N(2)	2.0736(17)
Fe(1)-N(4)#1	2.3110(18)	Fe(1)-Cl(1)	2.3933(6)
O(1)-Fe(1)-O(2)	101.00(6)	O(1)-Fe(1)-N(1)	89.40(6)
O(1)-Fe(1)-N(2)	166.85(6)	O(1)-Fe(1)-N(4)#1	87.09(6)
O(1)-Fe(1)-Cl(1)	95.59(5)	O(2)-Fe(1)-N(1)	166.84(6)
O(2)-Fe(1)-N(2)	90.00(6)	O(2)-Fe(1)-N(4)#1	84.38(6)
O(2)-Fe(1)-Cl(1)	94.03(5)	N(1)-Fe(1)-N(2)	78.76(7)
N(1)-Fe(1)-N(4)#1	88.16(7)	N(1)-Fe(1)-Cl(1)	92.95(5)
N(2)-Fe(1)-N(4)#1	86.83(7)	N(2)-Fe(1)-Cl(1)	90.77(5)
N(4)#1-Fe(1)-Cl(1)	177.11(5)		

Symmetry transformations used to generate equivalent atoms: #1 $x-1/2, y, -z+1/2$; #2 $x+1/2, -y+1/2, -z+1$ for **1**. #1 $x+1/2, y, -z+3/2$; #2 $-x+1, -y+1, -z+1$; #3 $x-1/2, -y+3/2, -z+1$ for **2**.

Table S3. Hydrogen bonding data of **1** and **2**.

1				
<i>D</i> -H··· <i>A</i>	<i>d</i> (<i>D</i> -H) (Å)	<i>d</i> (H··· <i>A</i>) (Å)	<i>d</i> (<i>D</i> ··· <i>A</i>)(Å)	<i>D</i> -H··· <i>A</i> (°)
C(15)-H(15)···Cl(1)	0.95	2.66	3.5871(5)	165
C(20)-H(20)···Cl(1)	0.95	2.74	3.6680(5)	165
2				
<i>D</i> -H··· <i>A</i>	<i>d</i> (<i>D</i> -H) (Å)	<i>d</i> (H··· <i>A</i>) (Å)	<i>d</i> (<i>D</i> ··· <i>A</i>)(Å)	<i>D</i> -H··· <i>A</i> (°)
C(5)-H(5)···Cl(1)	0.93	2.81	3.7166(2)	164
C(7)-H(7)···Cl(1)	0.93	2.81	3.7120(2)	163

Table S4. Comparison of the photocatalytic CO₂ reduction activities with varied photocatalysts.

Photocatalyst	Products	CO formation rate ($\mu\text{mol g}^{-1} \text{h}^{-1}$)	Ref.
1	CO	14.3	This work
2	CO	31.6	This work
NH ₂ -MIL-53(Fe)	CO	3.1	S1
NH ₂ -MIL-88B(Fe)	CO	10.3	S1
NH ₂ -MIL-101(Fe)	CO	17.5	S1
UiO-68-NH ₂	CO	2.19	S5
Pt(2)@NH ₂ -UiO-68	CO	66.7	S6

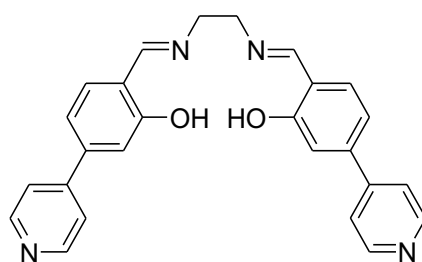


Fig. S1. Structure of organic ligand H₂L.

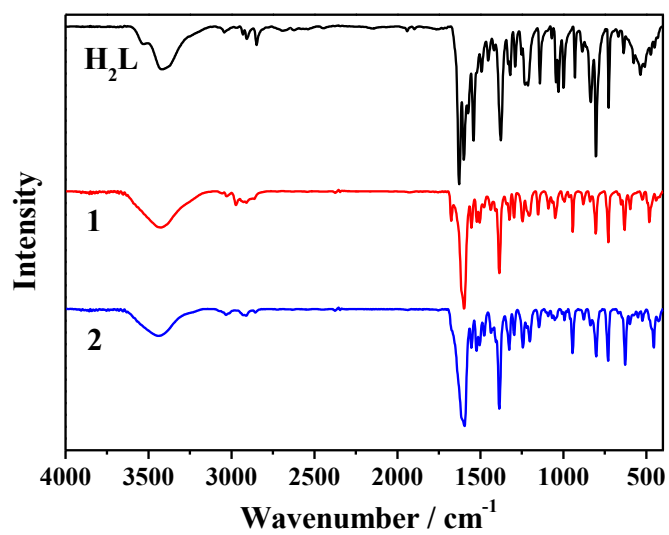


Fig. S2. IR spectra of H₂L, **1** and **2**.

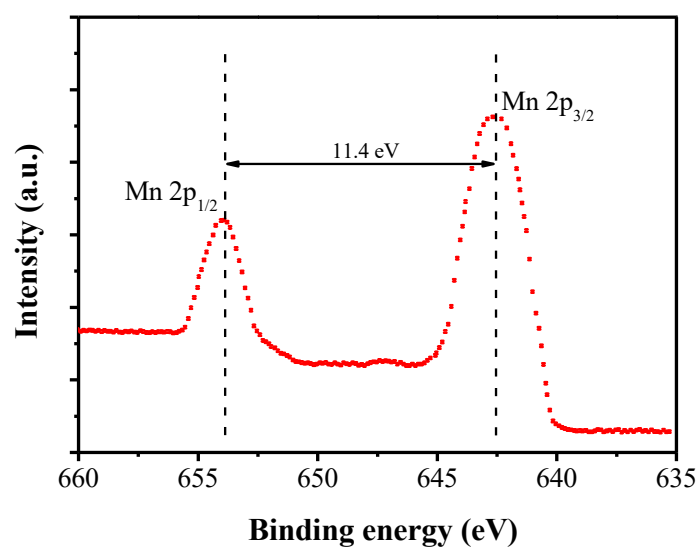
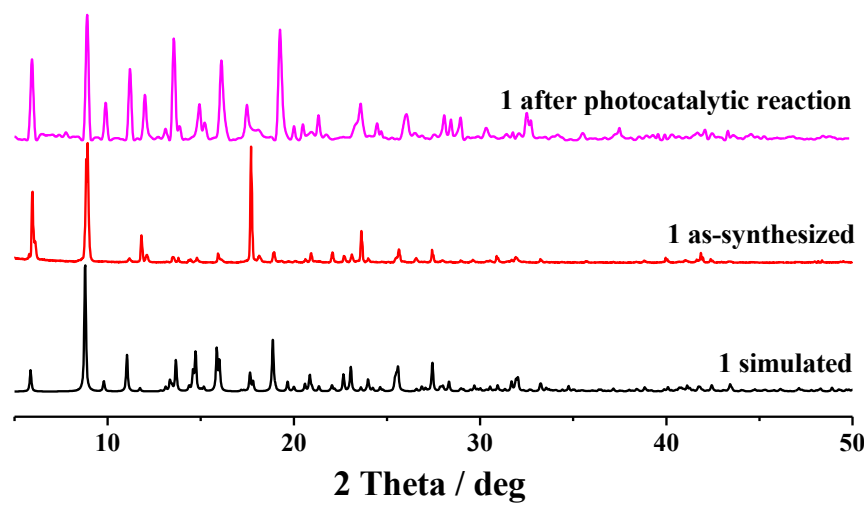
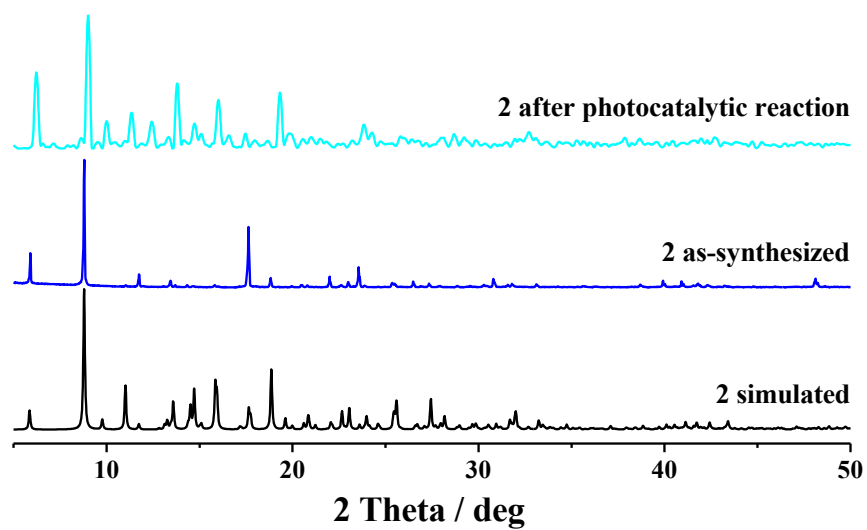


Fig. S3. XPS spectrum of Mn 2p in **1**.



(a)



(b)

Fig. S4. PXR D patterns of **1** (a) and **2** (b).

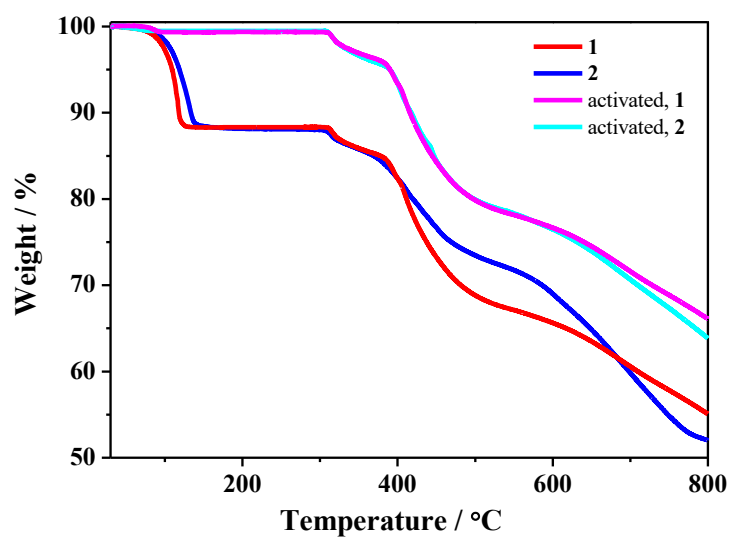


Fig. S5. TGA of 1 and 2.

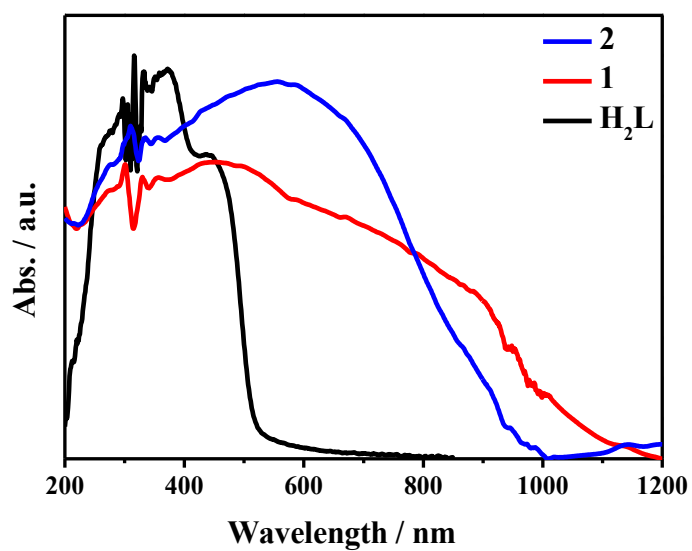


Fig. S6. UV-Vis spectra of H₂L, 1 and 2 in the solid state at room temperature.

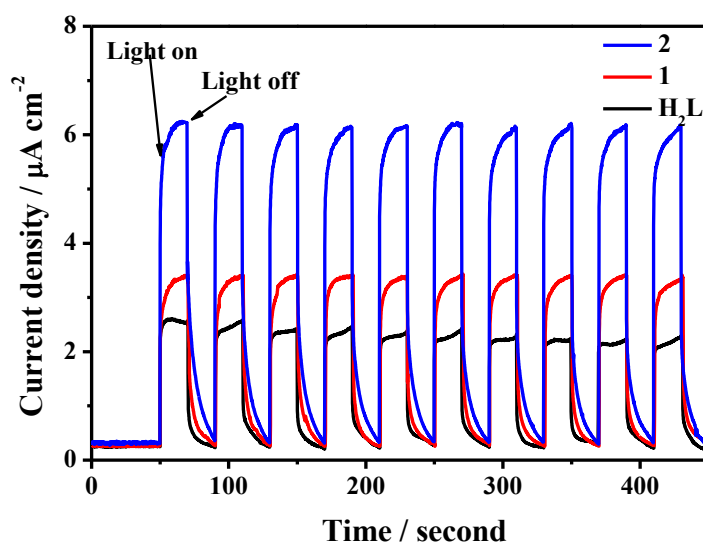
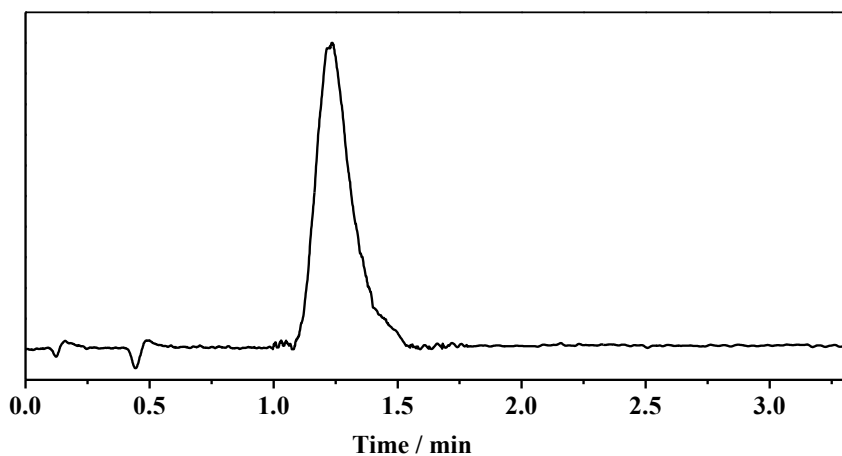
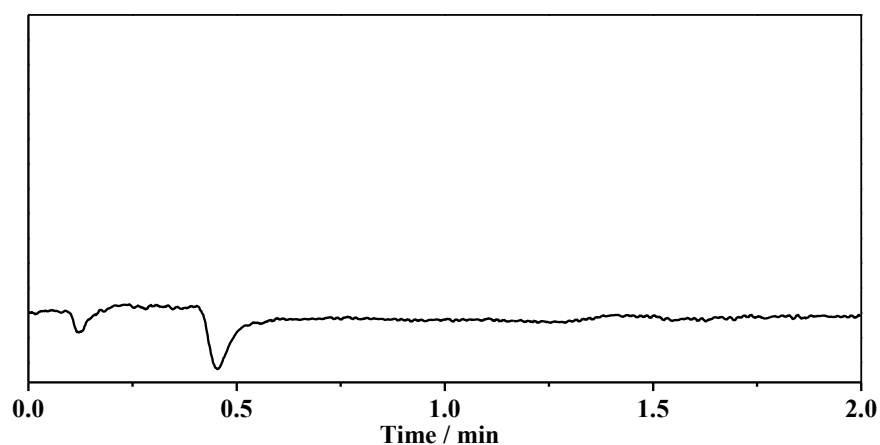


Fig. S7. Photocurrent responses of H₂L, 1 and 2.

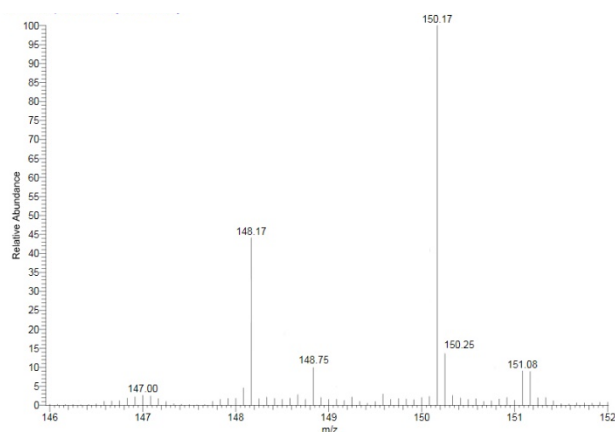


(a)

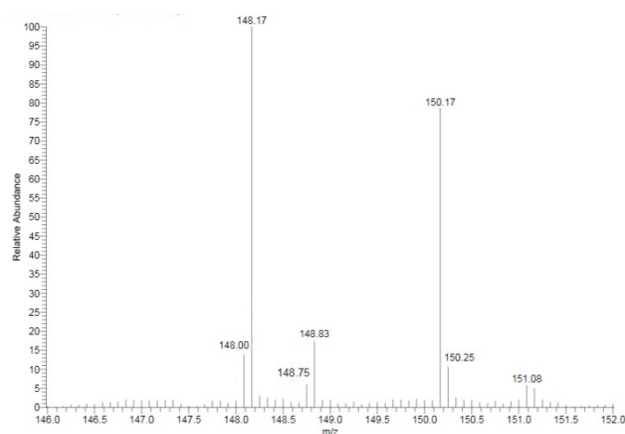


(b)

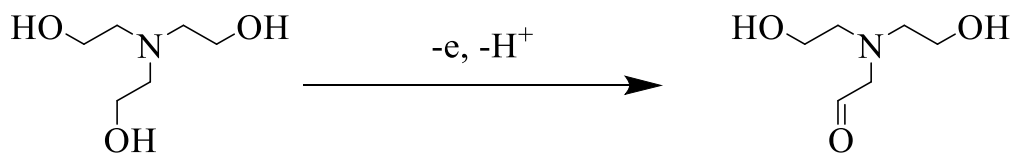
Fig. S8. Typical gas chromatogram observed during long-term irradiation: (a) FID detector for CO and CH₄ monitoring, CO was detected with retention time of about 1.290 min, however, no CH₄ (retention time: 2.540 min) was detected; (b) TCD detector for H₂ detecting, which showed no H₂ (retention time: 0.578 min) was detected.



(a)



(b)



(c)

Fig. S9. ESI-MS spectra for TEOA after reaction for 3 (a) and 6 (b) hours. (c) The possible product of TEOA.

Notes: ESI-MS spectroscopy was used to detect the possible product of TEOA. As shown in Fig. S9, there are two peaks around 148 and 150 assigned to the product of TEOA after reaction and TEOA. With the increase of the reaction times, the peak intensity of 148 becomes more and more strong. Based on the previous report,^{S7, S8} this peak of product could be assigned to an aldehyde, which arises as a result of TEOA oxidation.

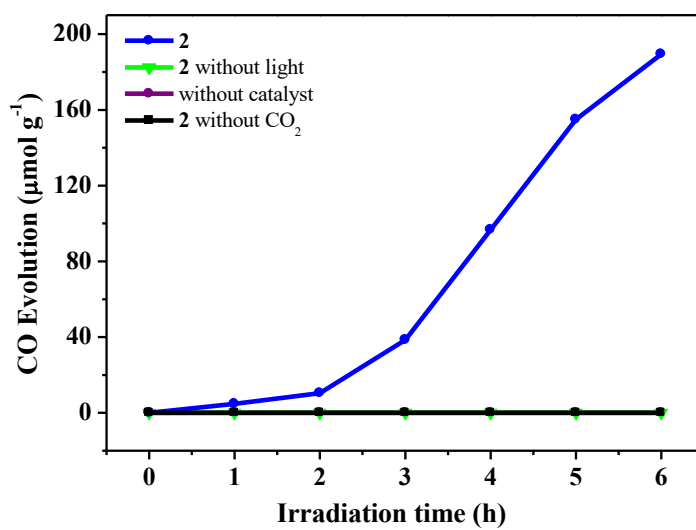


Fig. S10. Time dependent CO evolution over **2**, **2** without CO₂, **2** without light and without **2**.

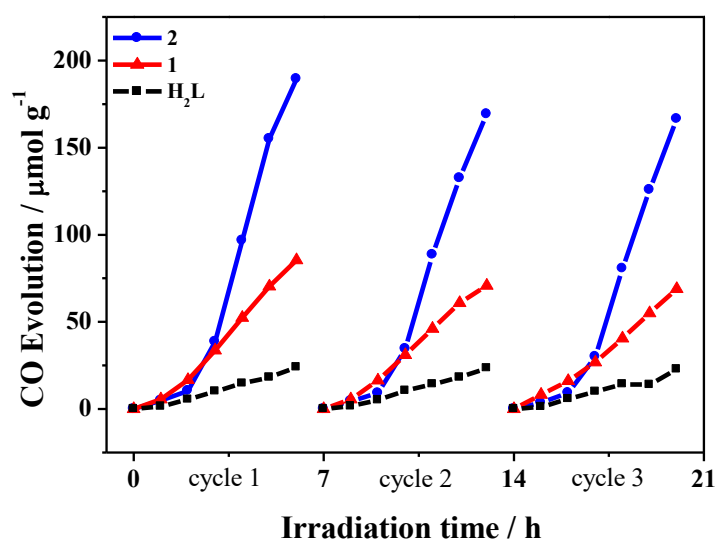


Fig. S11. Time dependent CO evolution over H₂L, **1** and **2** in 3 cycles.

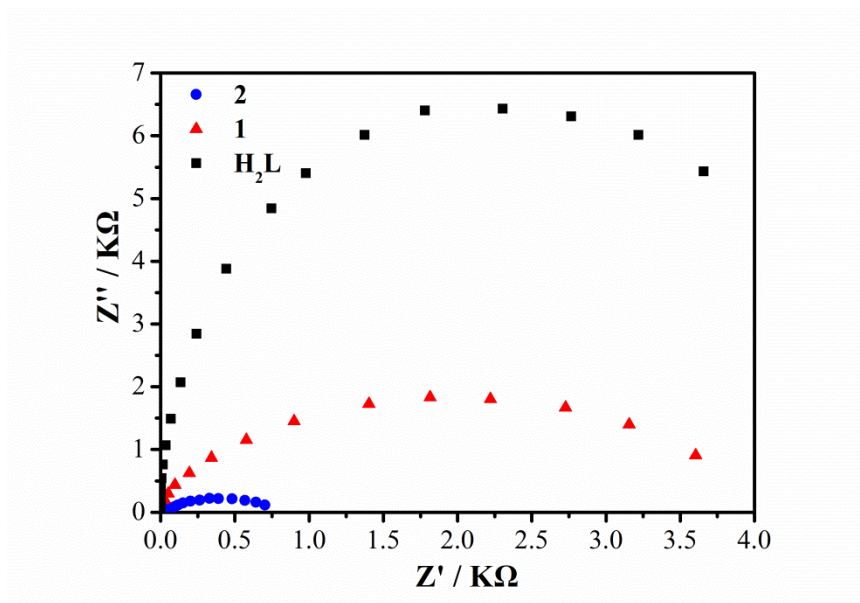


Fig. S12. EIS Nyquist plots of H₂L, **1** and **2**.

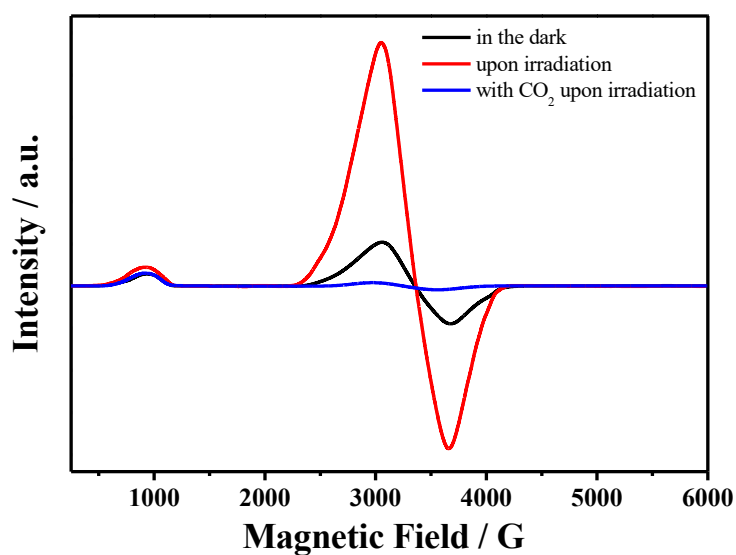
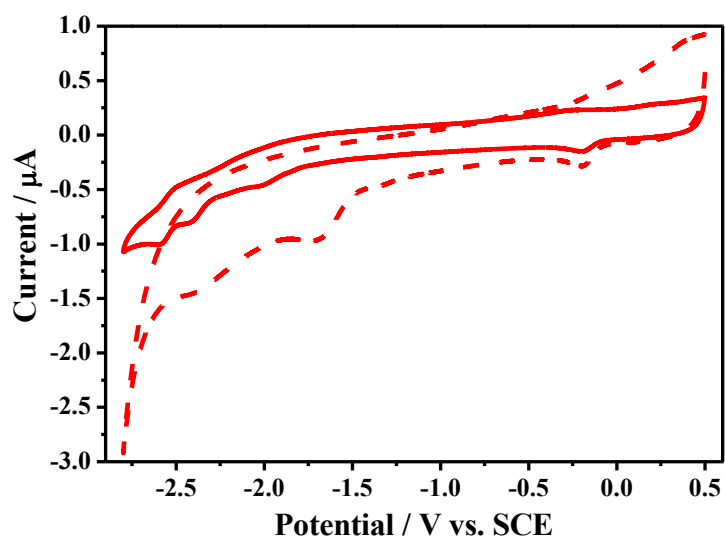
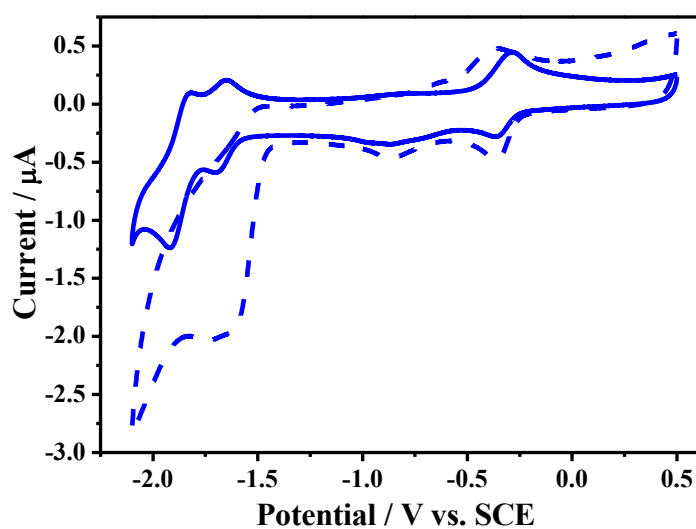


Fig. S13. X-Band (9.44 GHz) CW EPR spectra of a mixture of **1** with TEOA: in the dark (black); upon irradiation (red); in the presence of CO₂ upon irradiation (blue).

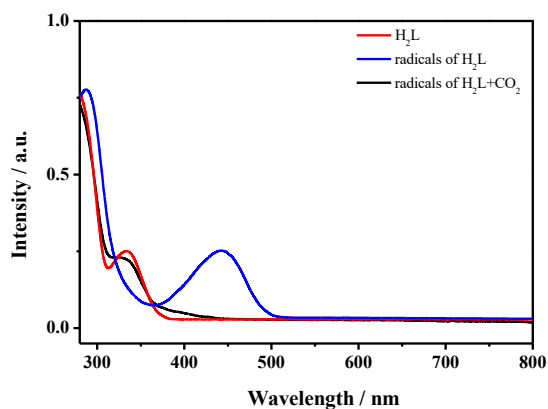


(a)

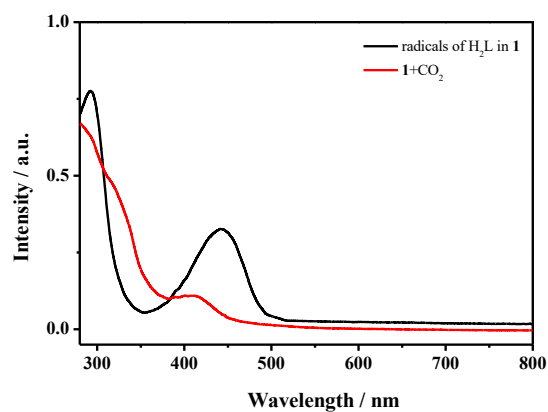


(b)

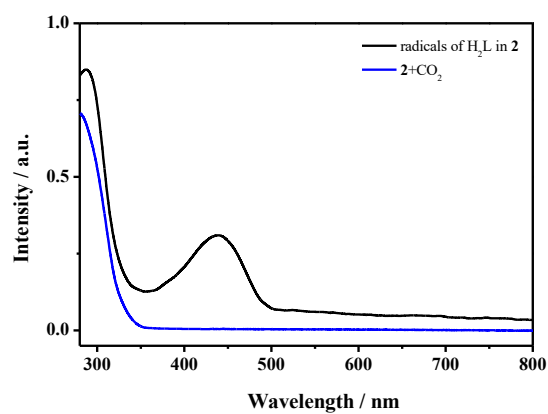
Fig. S14. CV (solid line, 1 mM catalyst in DMF + 0.1 M $n\text{-Bu}_4\text{NPF}_6$ at 0.1 V/s; dashed line, 1 mM catalyst in DMF + 0.1 M $n\text{-Bu}_4\text{NPF}_6$ in the presence of 0.23 M CO_2 at 0.1 V/s) of (a) **1** and (b) **2**.



(a)

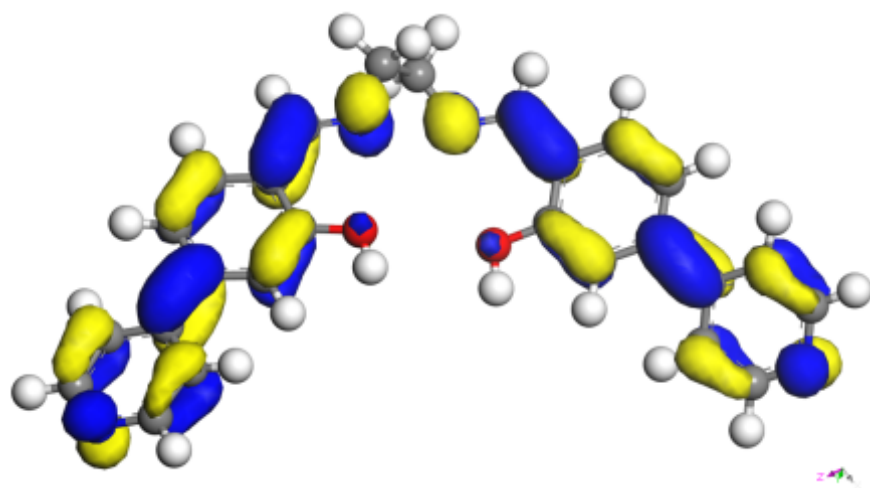


(b)

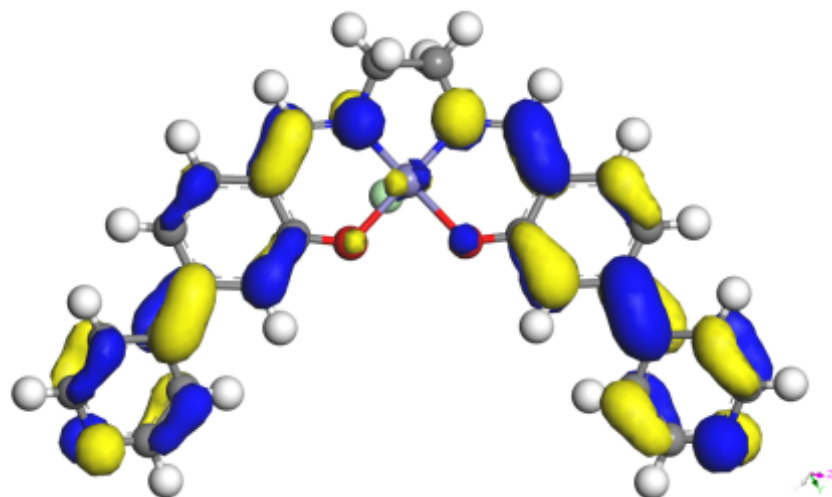


(c)

Fig. S15. UV-vis spectral changes upon electrochemical reduction of (a) H_2L , (b) **1** and (c) **2** in DMF at 298 K. Conditions: 1×10^{-4} M; 0.10 M tetrabutylammonium hexafluorophosphate; supporting electrolyte; controlled-potential reduction at -2.00 V vs SCE.



(a)



(b)

Fig. S16. DFT Calculated HOMO of (a) H₂L and (b) 1.

Reference

- [S1] X. Y. Dao, J. H. Guo, Y. P. Wei, F. Guo, Y. Liu and W. Y. Sun, *Inorg. Chem.*, 2019, **58**, 8517-8524.
- [S2] G. M. Sheldrick, *SADABS, Program for Empirical Adsorption Correction of Area Detector Data*, University of Göttingen: Germany, 2003.
- [S3] G. M. Sheldrick, *SHELXS-2014, Program for the Crystal Structure Solution*, University of Göttingen: Germany, 2014.
- [S4] G. M. Sheldrick, *SHELXL-2018, Program for the Crystal Structure Refinement*, University of Göttingen: Germany, 2018.
- [S5] Y. P. Wei, Y. Liu, F. Guo, X. Y. Dao and W. Y. Sun, *Dalton Trans.*, 2019, **48**, 8221–8226.
- [S6] F. Guo, Y. P. Wei, S. Q. Wang, X. Y. Zhang, F. M. Wang and W. Y. Sun, *J. Mater. Chem. A* 2019, **7**, 26490 - 26495.
- [S7] H. Zhang, J. Wei, J. Dong, G. Liu, L. Shi, P. An, G. Zhao, J. Kong, X. Wang, X. Meng, J. Zhang and J. Ye, *Angew. Chem. Int. Ed.*, 2016, **55**, 14310-14314.
- [S8] M. Elcheikh Mahmoud, H. Audi, A. Assoud, T. H. Ghaddar and M. Hmadeh, *J. Am. Chem. Soc.*, 2019, **141**, 7115-7121.